Water Air Soil Pollut (2015) 226:83
DOI 10.1007/s11270-015-2355-0

Enhanced Adsorptive Removal of Methylene Blue from Aqueous Solution by Alkali-Activated Palygorskite

Wenbo Wang · Fangfang Wang · Yuru Kang · Aiqin Wang

Received: 25 November 2014 / Accepted: 6 February 2015

Abstract Silicate clay materials are promising natural adsorbents with abundant, low cost, stable, and eco-friendly advantages, but the limited adsorption capacity restricts their applications in many fields. Herein, palygorskite (PAL) was facilely activated with alkali to enhance its adsorptive removal capability for methylene blue (MB). The effects of alkali activation on the microstructure, physicochemical, and adsorption properties of PAL for MB were intensively investigated. It was found that the moderate alkali activation can partially remove the metal cations (i.e., Al^{3+}, Mg^{2+}) and Si in the crystal backbone of PAL by which new "adsorption sites" were created and the surface negative charges increased. The adsorption capacity and rate of PAL for MB were evidently enhanced due to the effective activation. The adsorption isotherms were described by Freundlich isotherm model very well, and the adsorption kinetics can be accurately presented by a pseudo-second-order model. It can be inferred from the fitting results that the overall adsorption process was controlled by external mass transfer and intra-particle diffusion (the dominant role). The multiple adsorption interactions (hydrogen bonding, electrostatic interactions, mesopore filling, and complexing) were turned out to be the dominant factors to improve the adsorption properties. It was revealed that the activated PAL could be used as a potential adsorption candidate for environmental applications.

Keywords Palygorskite · Alkali activation · Adsorption · Methylene blue

W. Wang · F. Wang · Y. Kang · A. Wang (✉)
R&D Center of Xuyi Attapulgite Applied Technology, Lanzhou Institute of Chemical Physics, Chinese Academy of Sciences, Xuyi 211700, China
e-mail: aqwang@licp.cas.cn

W. Wang · A. Wang
Key Laboratory for Palygorskite Science and Applied Technology of Jiangsu Province, Huaiyin Institute of Technology, Huai'an 223003, China

1 Introduction

Toxic dye effluents discharged from the textile, rubber, leather, and plastic industries pose a detrimental risk to human health, living organisms, and ecosystem, and so, to efficiently eliminate the dye pollutants from wastewater by employing an economical way becomes very urgent and attracts worldwide attention (Wan Ngah et al. 2011; Szabó et al. 2014). Adsorption has been recognized as one of the most promising ways to remove various pollutants because it is simple, highly efficient, easily to be operated, and low cost. Also, the adsorbents can be facilely designed at molecular level according to the structure or type of pollutants, and a variety of adsorbents have been developed for meeting different application requirements (Kumar et al. 2013; Zhang et al. 2013; Wang et al. 2013; Çöle et al. 2013).

Silicate clay minerals with abundant, nontoxic, stable, low cost, and eco-friendly advantages have been frequently used as naturally available materials for the efficient removal of pollutants (Olu-Owolabi et al. 2010; Liu et al. 2012; Sotelo et al. 2013; Papoulis et al. 2013a,

Published online: 27 February 2015

b; Wang et al. 2014). As a special member in the family of silicate minerals, PAL has received more attention as an adsorbent due to its unique structure features. It is a one-dimensional nanorod-like hydrated Mg-rich silicate clay mineral with the theoretical formula of $Si_8Mg_5O_{20}(OH)_2(H_2O)_4{\cdot}4H_2O$ (Bradley 1940). It contains continuous tetrahedral sheets but discontinuous octahedron sheets, in which the apical oxygen atoms of tetrahedron point away from the basal oxygen atom plane in opposing directions at regular intervals and coordinate with octahedral cations to form talc-like 2:1 ribbons. Each ribbon alternately arranges to form interfingering nanosized channels (0.37 nm × 0.64 nm) along the fiber axis (Galan 1996). The intrinsic structure characters of PAL make it possessing larger specific surface area, plentiful surface groups, negative surface charges, higher surface energy, and cation exchange capacity (Ruiz-Hitzky et al. 2013; Papoulis et al. 2013b; Xu et al. 2014). So, many small organic molecules (Sarkar et al. 2012), dyes (Al-Futaisi et al. 2007; Frost et al. 2010; Liu et al. 2012) and heavy metal ions (Middea et al. 2013) could easily interact with PAL through different action forces such as the Van der Waals' force, electrostatic attraction, hydrogen bonding association, or ion exchange and thus being adsorbed on the surface of PAL or entered into its pores. Hence, the adsorption capability of PAL is highly dependent on the strength of the interaction forces occurred on the contact interface, and it could also be well controlled by altering the microcosmic crystal structure and surface characters.

It could be found from the crystal structure of PAL that although there are numerous tunnels in the PAL rods, the cross-sectional area of the tunnel is only 0.37 × 0.64 nm^2, which means that the bigger dye molecules usually fail to enter the inside tunnels (Sánchez del Río et al. 2009). In this case, the tunnels may only contribute little to the adsorption process of dyes. Our previous work (Zhang et al. 2015) also found that the Mg-rich PAL has poor adsorption capacity for dye though it has relatively greater specific surface area. The main reason is that the number of octahedral cations is 5 and Mg(II) thoroughly occupied the octahedral sites, with no obvious defect in crystal structure (Post and Heaney 2008), whereas the Mg-poor PAL is more favorable to adsorb MB dye due to the existence of moderate defects in the crystal. Besides, the substitution or deficiency degree of octahedral cations mainly determines the magnitude of negative surface charges. The intrinsic negative surface charges of PAL make it easily to adsorb cationic dyes by electrostatic interaction, and the charges may have more obvious influence on the adsorption process. All these researches come down to the point that the creation of moderate defects in the PAL crystal is the key to build new "adsorption sites," enhance the surface charges, and improve the adsorption properties.

Acid treatments have been frequently used to improve the adsorption properties of clay minerals by producing new porosity, active Si–OH groups, and acidic sites and increasing surface activity (Gonzalez et al. 1990; Chen et al. 2007). The leaching of partial Mg^{2+} or Al^{3+} in the crystal backbone of clay minerals under moderate acid attack may create new "cavity," which facilitate to enhance the adsorption or decoloring properties of PAL (Jozefaciuk and Bowanko 2002; Frini-Srasra and Srasra 2010). However, acid treatment does not dissolve Si though it is inclined to remove Mg^{2+} or Al^{3+} (Barrios et al. 1995; Zhang et al. 2010). Comparatively, alkali has stronger corrosion capability to not only the metal cations, but also the Si–O–Si bonds (White et al. 2012). It may create many new Si–O^--"active sites" by breaking the inert Si–O–Si bonds. Consequently, the simple alkali activation may be effective to optimize the structure of PAL and enhance its adsorption properties for cationic dyes.

Here, the effects of alkali activation on the structure and morphology of PAL were systematically studied by combining the X-ray diffraction (XRD), scanning electronic microscopy (SEM), transmission electron microscopy (TEM), Fourier transform infrared spectroscopy (FTIR), N_2 adsorption–desorption, and zeta potential analyses, and the adsorption behaviors of the activated PAL for MB dye were evaluated in detail.

2 Experimental

2.1 Materials

PAL clay mineral comes from Mingguang Mine located at Mingguang city of Anhui province, China. It was pretreated by rolling for one time. Sodium hydroxide (NaOH, AR grade) and methylene blue (MB, AR grade) were purchased from Sinopharm Chemical Reagent Co., Ltd (Shanghai, China). All other reagents are of analytical grade, and all solutions were prepared with de-ionized water.

2.2 Activation of PAL with NaOH Solution

Pretreated PAL clay (5 g) was dispersed in 70 mL of NaOH solution with various concentrations (0, 0.5, 1.0, 2.0, 3.0, and 5.0 mol/L) under mechanical stirring at 800 rpm to form a homogeneous suspension. After being stirred for 4 h, the solid product was separated by centrifuging at 5000 rpm, fully washed with deionized water, and then dried at 105 °C for 4 h. The dried product was ground and passed through a 200-mesh sieve for further use. The obtained samples were marked as N-x (x represents the concentration of NaOH solution).

2.3 Adsorption Experiments

Adsorption experiments were performed by the following procedure: 50 mg of PAL samples was mixed with 25 mL of MB solution and fully agitated in a thermostatic shaker (THZ-98A) at 120 rpm and 30 °C for 4 h to reach adsorption equilibrium. The solution was instantly separated from the adsorbent using a 0.22-μm filter, and the concentration of MB in the percolate was determined using a UV–vis spectrograph at the maximum absorbance wavelength of 664 nm. The adsorption capacity of PAL for MB could be calculated using Eq. 1.

$$q = (C_0 - C_e)V/m \quad (1)$$

Here, q is the adsorption amount of PAL for MB at time t (q_t, mg/g) or at equilibrium (q_e, mg/g), V is the volume of MB solution used (mL), C_0 and C_e are the initial and final concentrations of MB (mg/L), and m is the mass of PAL sample (mg). In order to study the adsorption isotherms, the adsorption properties of PAL for MB were evaluated in a set of MB solutions with different initial concentrations from 50 to 1200 mg/L (pH 7). The effect of pH values on adsorption properties was evaluated by adjusting the pH value of MB solution (initial concentration is 200 mg/L) to 3, 4, 5, 6, and 7, respectively. For each test, the adsorption capacities could be calculated using Eq. (1). All experiments were parallel carried out for three times, and the averages are reported.

The dynamic adsorption behaviors were evaluated according to the following procedure: 25 mL of the MB solution with the initial concentration of 200 or 800 mg/L and pH 7 was fully contacted with 25 mg of PAL sample, and then, the solution was separated from the solid by a filtering process at the set time intervals (300–7200 s). The adsorption capacities of PAL for MB at each moment can be calculated by using Eq. (1).

2.4 Characterizations

FTIR spectra are measured on a Thermo Nicolet NEXUS™ spectrophotometer in the range of 4000–400 cm^{-1} using a KBr platelet. The morphology of sample is observed using a JSM-6701F field emission scanning electron microscope (FESEM, JEOL, Ltd. Japan) after fixing the samples on copper stubs and coating with gold film. TEM image is taken using a JEM-1200 EX/S transmission electron microscope (TEM) (JEOL, Tokyo, Japan). The XRD patterns are collected on an X'Pert PRO diffractometer equipped with a Cu Kα radiation source (40 kV, 40 mA). The specific surface area is determined by the N_2 adsorption–desorption isotherms at 77 K with the ASAP 2010 analyzer (Micromeritics, USA). The values of specific surface area (S_{BET}) are calculated by the Brunauer–Emmett–Teller (BET) equation. The total pore volumes (V_{total}) are obtained from the volume of liquid N_2 held at the relative pressure P/P_0=0.95. The micropore volume (V_{micro}) is estimated by the t-plot method. The chemical composition is determined using a Minipal 4 X-ray fluorescence spectrometer (PANalytical, Netherland). Zeta potentials are measured on a Malvern Zetasizer Nanosystem with irradiation from a 633-nm He–Ne laser (ZEN3600).

3 Results and Discussion

3.1 Microstructure and Physicochemical Properties

As is shown in Fig. 1, the alkali treatment has obvious effect on the morphology of PAL rods. The length and aggregation state of PAL rods do not evidently change after being activated with NaOH solution when the concentration is lower (≤0.5 mol/L) (Fig. 1b), whereas the length of rods slightly reduces and the rods are inclined to aggregate with each other when the NaOH concentration increases to 1.0 mol/L. The reduction of length of rods and the aggregation tend to be more obvious with further increasing the concentration to 3 mol/L, but the shape of rods is still remained. Intriguingly, the rod-like shape of PAL disappears when the concentration of NaOH solution is 5.0 mol/L, and only a

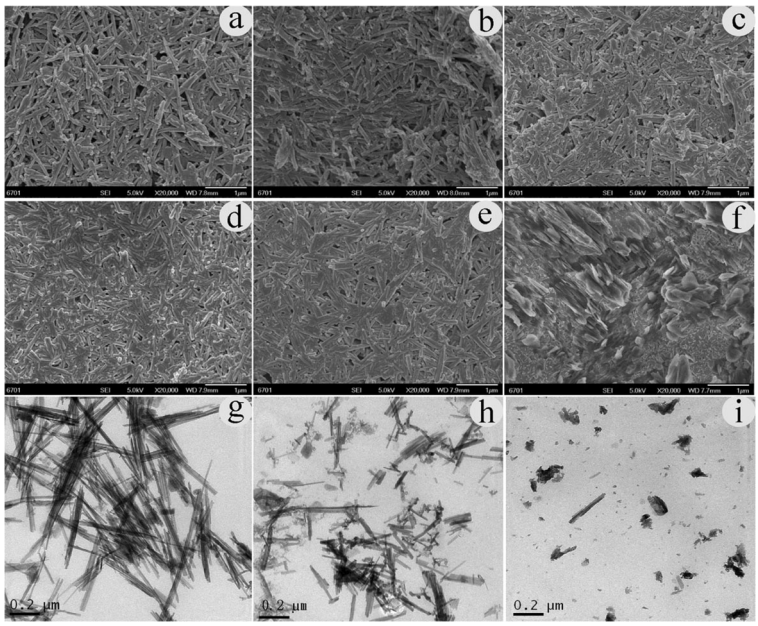

Fig. 1 FESEM micrographs of **a** N-0, **b** N-0.5, **c** N-1, **d** N-2, **e** N-3, and **f** N-5 and TEM micrographs of **g** N-0, **h** N-3, and **i** N-5

coarse, gap- and drape-shape surface morphology could be observed. The same change tendency is also observed in the TEM image (Fig. 1i). These apparent changes give visual information that the ribbon-layer texture composed of continuous silicon–oxygen tetrahedron and discontinuous Mg(Al)–oxygen octahedron may be partially or thoroughly destroyed after being treated with NaOH solution, and the structure or morphology could be controlled by adjusting the concentration of NaOH solution. The low concentration of NaOH solution (≤0.5 mol/L) may be helpful to activate the surface of PAL rods, with no the change of crystal structure; the moderate concentration of NaOH solution (<5.0 mol/L) may simultaneously activate the surface and remove some cations in the octahedron sheets to slightly change the structure; the concentrated alkaline is devastating to the crystal structure. These results show a good fit to the prediction that alkali treatment has a controllable leaching effect on the metal cations and Si components in the crystal backbone of clay (Jozefaciuk and Matyka-Sarzynska 2006; White et al. 2012) and will be effective to create active sites in the crystal texture. The microstructure change caused by leaching effect could be observed more clearly from the TEM image of N-3 (Fig. 1h), with the appearance of some small fragments around the nanorods. Also, it was directly proved by the change of chemical composition.

The chemical composition of PAL samples was determined by X-ray fluorescence (XRF) analysis. As is shown in Fig. 2, the content of Al_2O_3 gradually decreases from 8.19 to 7.37 % (the decreasing ratio is 10.01 %), whereas the content of MgO only slightly decreases from 12.66 to 11.98 % (the decreasing ratio is 5.37 %) with increasing the concentration of NaOH solution from 0 to 3.0 mol/L. In PAL, the Mg and Al ions are mainly located in the octahedron sheet, in which Mg occupies M3 sites and Al and Fe occupy M2 sites (Post and Heaney 2008). After alkali treatment, the Al content decreases more obviously than Mg content despite that the number of Mg is dominant in octahedron sheet, which implies that Al ions are easily to be leached than Mg under alkali attack. Corresponding to the change of Mg and Al ions, the content of SiO_2 decreases from 51.44 to 45.7 % (the decreasing ratio is 11.16 %) in the same concentration range, which is different from the case of acid treatment that the SiO_2 content only changes a little (Zhang et al. 2010). What is matter is that being different from acid activation, some amorphous SiO_2 or SiO_4 is simultaneously dissolved during the alkali activation process. The Si–O–Si bonds may be broken under alkaline condition as described in the Eqs. (2) and (3) (Golden et al. 1985). By comparison with Al, Mg, and Si elements, the change of content of CaO, K_2O, and Fe_2O_3 is relatively smaller. When the concentration of NaOH solution increases to 5.0 mol/L,

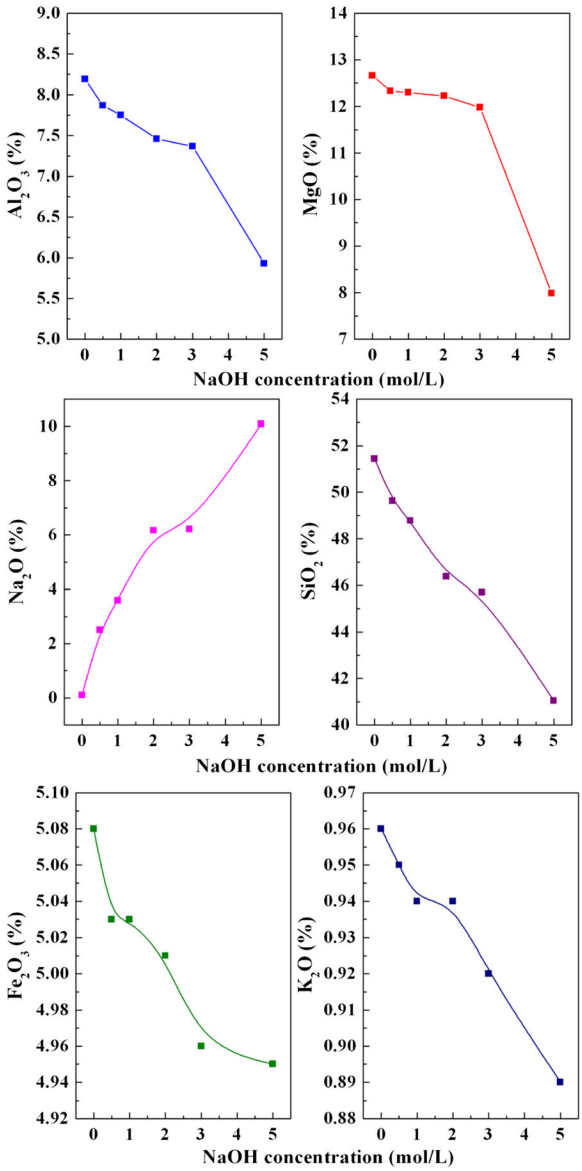

Fig. 2 Variation of chemical composition with increasing the concentration of NaOH solution

the contents of Al_2O_3, MgO, and SiO_2 decrease to 5.93, 7.8, and 41.4 %, which indicate that many Al^{3+}, Mg^{2+}, ions and Si^{4+} are disassociated from the backbone, and the crystal structure of PAL collapsed.

$$Si–O–Si + OH^- \rightarrow Si–O^- \quad (2)$$

$$Si–O–M + OH^- \rightarrow Si–O^- + M–O^- \quad (3)$$

The XRD analyses are very effective to confirm the change of crystal structure. As can be seen from Fig. 3, a

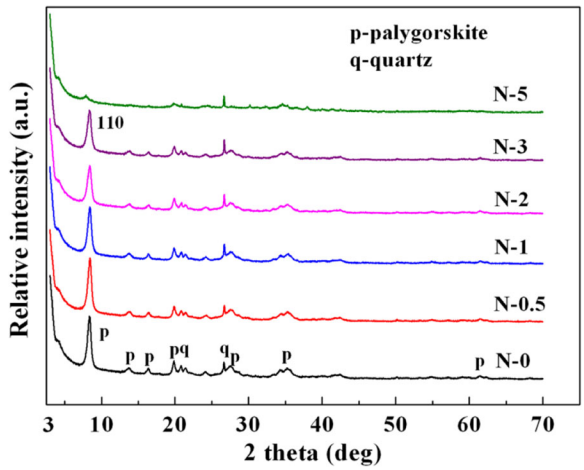

Fig. 3 XRD patterns of raw PAL and alkali-activated PAL

stronger (110) diffraction peak at $2\theta=8.39°$ ($d=1.0530$ nm) was observed in the diffraction pattern of raw PAL. The position and intensity of this peak have no obvious change after being treated with low concentration of NaOH solution (0.5 mol/L), but they gradually decrease with increasing the concentration from 0.5 to 3.0 mol/L. The decrease of peak intensity is resulting from the partial leaching of metal ions (Fig. 2) from the octahedron sheets under the action of alkali attack. Nonetheless, the (200) diffraction peak at $2\theta=13.69°$ (corresponding to the SiO_4 tetrahedron sheets) and (240) diffraction peak at $2\theta=24.19°$ (corresponding to the octahedron sheets) (Liu et al. 2013) only slightly weakened with increasing the concentration of NaOH solution to 3 mol/L, indicating that the tetrahedron and octahedron skeleton of PAL still remained despite the leaching of some metal ions. The situation would be very different, however, if the concentration of NaOH solution is above 5 mol/L. It is obvious that the (110) diffraction peak greatly weakens and shifts to $2\theta=7.99°$ and while the (200) and (240) diffraction peaks disappear along with the change of (110) diffraction peak. It was revealed that the octahedron cations and tetrahedron Si tend to be excessively leached by stronger alkali, which results in the collapse or reconstruction of crystal structure of PAL. What is more, it is worth noting that the alkaline activation of PAL is mainly a controllable bleaching process to crystal, instead of the transformation of crystal structure, because no new diffraction peak appears in the activation process despite that the (110) peak was decreased. The weaker diffraction peaks at $2\theta=20.8°$ and 26.6°, ascribed to the existence of small amount of quartz, have no obvious change after alkali

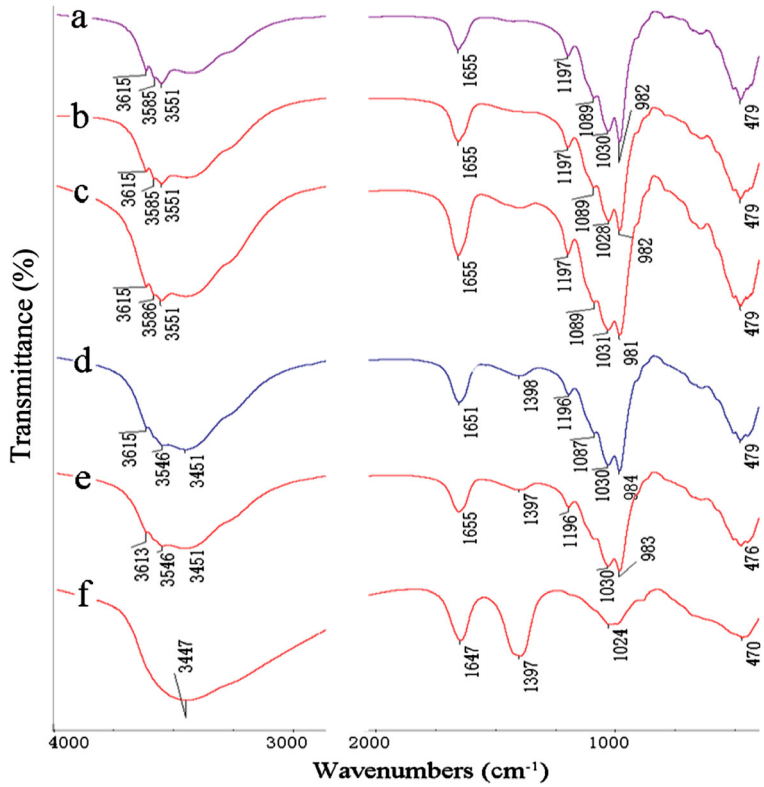

Fig. 4 FTIR spectra of N-0 (*a*), N-0.5(*b*), N-1 (*c*), N-2 (*d*), N-3 (*e*), and N-5 (*f*)

activation, indicating that the alkali activation does not affect the crystal structure of quartz.

As discussed above, the leaching of the octahedral metal ions or the tetrahedral Si in the PAL crystal means that more broken bonds may be generated during this process. FTIR spectra analyses are effective to describe the change of surface groups of PAL. As is shown in Fig. 4, the four shoulder bands at about 3615 cm^{-1} (stretching vibration of Al_2O–H), 3581 cm^{-1} (stretching vibrations of Al(Fe^{3+})O–H), and 3548 cm^{-1} (O–H stretching vibrations of structural OH_2) (Suárez and Garcia-Romero 2006; Yan et al. 2012) are weakened after being activated with NaOH solution (from 0.5 to 3.0 mol/L) and almost disappeared with further increas-

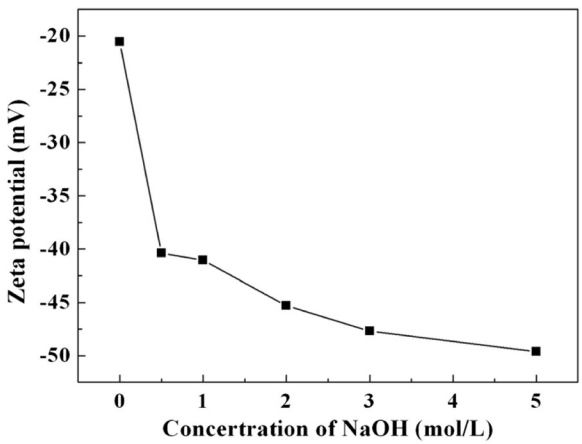

Fig. 5 Zeta potential of PAL treated with different concentrations of NaOH solution

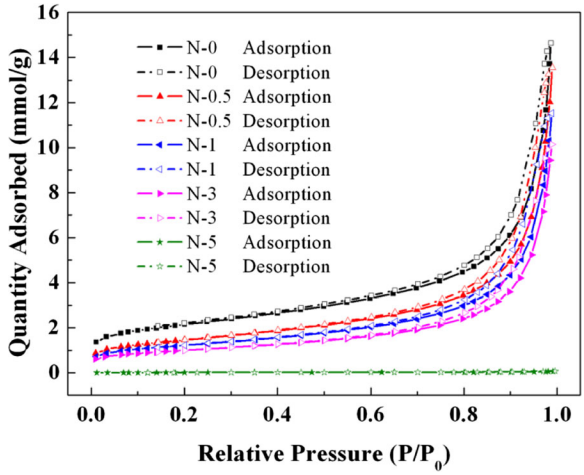

Fig. 6 N_2 adsorption–desorption isotherms of PAL before and after alkali treatment

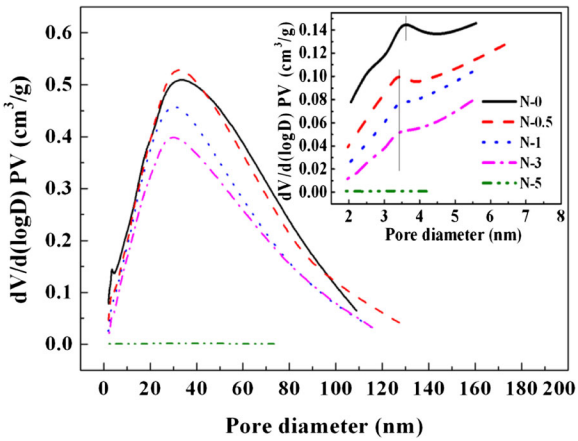

Fig. 7 Pore size distributions of PAL before and after alkali treatment

ing the concentration to 5.0 mol/L. The band at about 1196 cm^{-1}, ascribed to the stretching vibration of Si–O–Si that connects two reverse tetrahedron sheets, is the exclusive absorbance band of the ribbon-layer silicate. The band at 983 cm^{-1} is ascribed to the Si–O–M stretching vibration. The slightly decrease of the two bands with increasing the concentration of NaOH solution indicates that some Si–O–Si and Si–O–M bands were broken under the action of NaOH. With further increase of the concentration of NaOH solution (5.0 mol/L), however, these bands disappear due to the breakage of the crystal backbone of PAL. The band centered at 515 cm^{-1}, ascribed to the deformation of silicate–oxygen tetrahedral sheet and the bending vibration of Si–O–Si bonds (McKeown et al. 2002), has no obvious change, indicating that silicon–oxygen tetrahedron is relatively resistant to the etching effect of alkali.

In general, the breakage of Si–O–Si and Si–O–M bonds may generate more $Si–O^-$ groups, and the leaching of metal ions from the crystal backbone may affect the charge distribution of PAL. As can be seen from Fig. 5, the zeta potential of PAL becomes more negative after modified with NaOH solution, and the PAL activated with 5.0 mol/L of NaOH solution gives the highest negative potential of −50 mV. The above XRF analysis has confirmed that the Al^{3+} and Mg^{2+} ions were leached from the crystal and some Si–O–Si(M) bonds were broken (Golden et al. 1985), with numerous $–Si–O^-$ (Na^+, Mg^{2+}) bonds being formed during this process, which would lead to the increase of negative charges on the surface of PAL. Viewed from another perspective, alkaline activation has been proved to be a simple and effective protocol to increase the surface negative charges.

The change of crystal structure also can be attested from the changes of pore texture parameters. The N_2 adsorption–desorption isotherms of the PAL samples at 77 K are shown in Fig. 6. As can be seen, the PAL activated by lower concentration of NaOH solution (≤3.0 mol/L) shows type I and IV isotherms according to the IUPAC classification (Sing et al. 1985; Rouquerol et al. 1999). The adsorption amount of N_2 for each sample gradually increases at lower relative pressure (P/P_0<0.60), which indicates the presence of a small amount of micropores. The adsorption amount of N_2 sharply increases at the higher P/P_0 due to the capillary condensation of N_2 in the mesopores (and/or macropores) and its multilayer adsorption onto the mesopores and macropores. The H3-type hysteresis at higher relative pressure was observed, indicating the existence of mesopores and/or macropores (Sing et al. 1985; Bakandritsos et al. 2004), and the conclusion that the pores in the samples are narrow slit-like pores or aggregates of plate-like particle also can be drawn (Sing et al. 1985; Bu et al. 2010). For the PAL sample, the hysteresis loops at the relative pressure higher than 0.6 are very narrow, indicating that PAL has relatively broader pore size distribution with the inclusion of more mesopores and macropores.

The pore size distributions (PSDs) of mesopores for the activated PAL were calculated by Barret–Joyner–Halenda (BJH) method from the adsorption branches

Table 1 Textural parameter of alkali-activated PAL

Samples	S_{BET} (m^2/g)	S_{ext} (m^2/g)	S_{micro} (m^2/g)	V_{micro} (cm^3/g)	PZ (nm)	PV
N-0	170.65	134.7671	35.8818	0.0155	8.7362	0.3727
N-0.5	117.01	103.5731	13.4395	0.0052	10.7986	0.3159
N-1	97.98	86.3496	11.6253	0.0045	11.8250	0.2896
N-3	79.78	67.2854	12.4910	0.0052	12.4388	0.2481
N-5	2.03	1.5090	–	0.0003	6.6195	0.0017

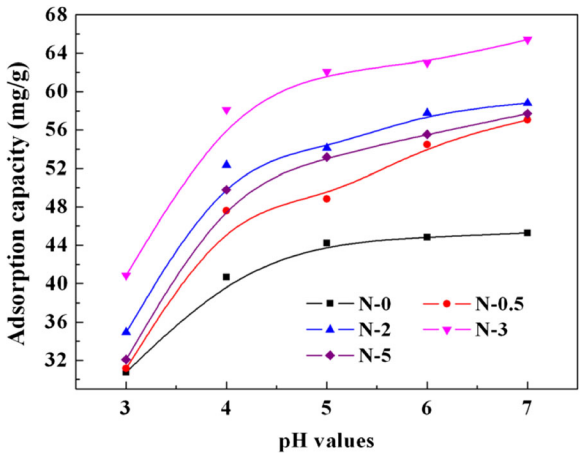

Fig. 8 Effect of pH on the adsorption capacity of PAL for MB (the initial concentration of MB is 200 mg/L, and the dosage of adsorbent is 1 g/L)

(Fig. 7) (Barrett et al. 1951). The corresponding PSD curve based on the BJH method (Fig. 7) exhibits two peaks: one is at 3.43~3.61 nm, which is ascribed to the tight stacking of PAL particles; the other is located at about 30.04~32.89 nm, which can be attributed to the aggregation of PAL rods (Al-Futaisi et al. 2007). After alkaline treatment, the PSD of PAL becomes broader in contrast to the untreated PAL. However, no N_2 adsorption–desorption behavior and distribution of pores are observed when the concentration of NaOH solution is 5.0 mol/L, which means that the pore texture has been destroyed by high concentration of NaOH solution (Table 1).

The specific surface area of PAL samples (170.65 m^2/g for N-0; 117.01 m^2/g for N-0.5; 97.98 m^2/g for N-1; 79.78 m^2/g for N-2; 2.03 m^2/g for N-5) decreases with increasing the concentration of NaOH solution, whereas the pore size (PZ) increases from 8.7362 nm (for N-0) to 10.7986 nm (for N-0.5), 11.8250 nm (for N-1), and 12.4388 nm (for N-3), but the

Scheme 1 Digital photos of MB solution before and after adsorption and the adsorption schematic of MB on PAL

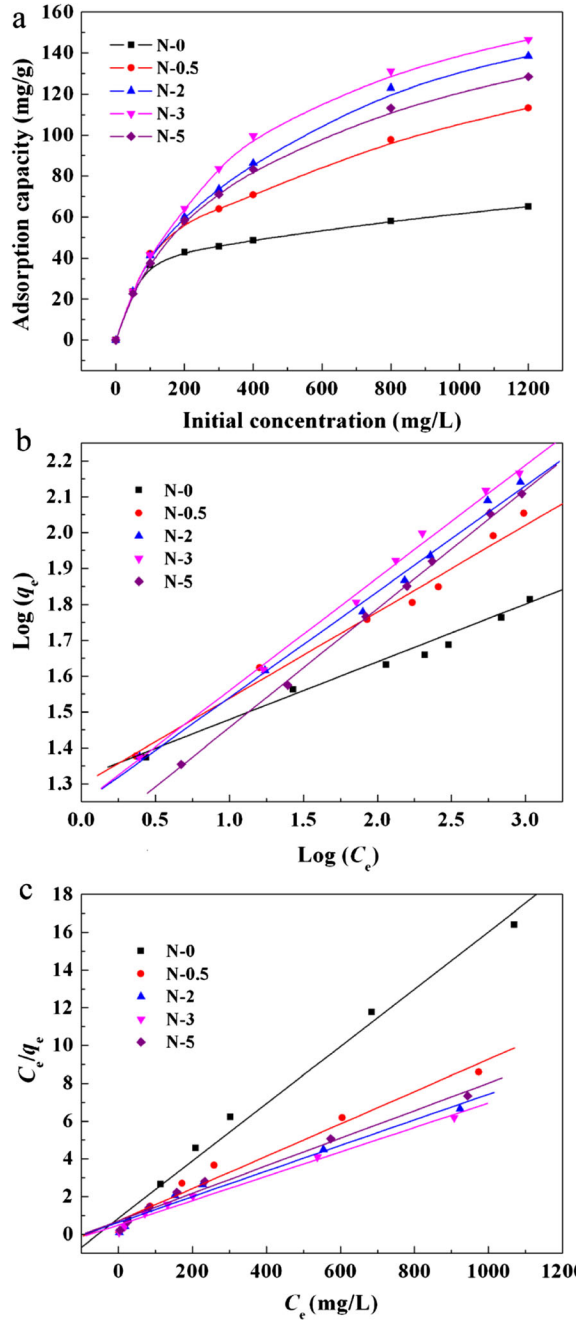

Fig. 9 Adsorption isotherm curves of PAL samples (**a**) and the fitting curves by the Freundlich isotherm model (**b**) and the Langmuir isotherm model (**c**)

micropore volume (V_{micro}) and pore volume (PV) were greatly reduced (see Table 1).

3.2 Adsorption Properties for MB

3.2.1 Effect of pH

Figure 8 shows the effects of pH on the adsorption of the PAL samples for MB. It can be seen that the adsorption capacity remarkably increased and then tends to be constant with increasing the pH values. The adsorption capacity of each sample follows the order of N-3 > N-2 > N-5 > N-0.5 > N-0. At lower pH value, the –Si–O^- groups exist in the form of –Si–OH and the main interaction between MB and PAL is hydrogen bonding. At higher pH, however, the –Si–OH will transform to –Si–O^-, and dominating interaction between MB and PAL would change to electrostatic forces. The latter force is much stronger than the former one, which is conductive to adsorption for cationic MB (Scheme 1). With increasing the pH value, the number of –Si–O^- groups increased, so the adsorption of cationic dye MB onto the negatively charged PAL is more favorable. The evident dependence of adsorption capacity on external pH values gives direct information that the electrostatic interaction is dominant to the adsorption process. Comparatively, the specific surface area may only have weaker influence on the adsorption capacity. As is discussed above, the specific surface area of alkali-activated PAL is smaller than that of N-0, and the specific surface area of N-5 is even close to zero. However, the adsorption capacity of N-0 is even lower than N-5, which reveals that specific surface area is not the dominant factor for the adsorption of MB.

3.2.2 Adsorption Isotherm

As shown in Fig. 9, the adsorption capacities of PAL samples for MB are sharply enhanced with increasing the initial concentration, because the driving force at the solid–liquid interface would be improved with the increase of initial dye concentration before the adsorption sites being saturated. Afterward, the increasing trend becomes flat and adsorption equilibrium is almost reached. In order to investigate the adsorption mechanism and characteristics of PAL for the dye removal (Grabowska and Gryglewicz 2007), the Freundlich (Eq. 4) (Freundlich 1906) and Langmuir (Eq. 5) (Langmuir 1918) isotherm models have been frequently introduced as follows.

$$\log q_e = \log K + (1/n)\log C_e \quad (4)$$

$$C_e/q_e = 1/(q_m b) + C_e/q_m \quad (5)$$

where q_e (mg/g) is the adsorption capacity of PAL samples for MB at equilibrium, C_e is the concentration of MB solution after adsorption (mg/L), q_m is the maximum adsorption capacity (mg/g), and b is the Langmuir adsorption constant (L/mg), which is related to the free energy of adsorption. K (L/g) and n (dimensionless) are the Freundlich isotherm constant and the heterogeneity factor, respectively. These parameters can be obtained by fitting the experimental data using the Langmuir (C_e/q_e vs C_e) and Freundlich ($\log q_e$ vs $\log C_e$) isotherm models (see Table 2). As can be seen, the linear correlation coefficient is R >0.9921 for the Freundlich isotherm model and R>0.9855 for the Langmuir model. This proves that the Freundlich isotherm model fits to

Table 2 Adsorption isotherm parameters for the adsorption of MB onto PAL

Samples	Langmuir equation			Freundlich equation		
	q_m (mg/g)	b (L/mg)	R	K	n	R
N-0	65.88	0.0179	0.9941	20.3437	6.2508	0.9922
N-0.5	116.69	0.0120	0.9855	19.5848	4.0771	0.9921
N-2	147.06	0.0108	0.9867	17.4137	3.3461	0.9965
N-3	154.56	0.0132	0.9934	17.4667	3.1532	0.9981
N-5	136.79	0.0103	0.9907	13.2520	2.9930	0.9995

adsorption data better than the Langmuir isotherm model. The 1/*n* is smaller than 1, which reveals a monolayer adsorption of MB. The applicability of Freundlich isotherm suggests that different sites with several adsorption energies are involved, and in some cases, the intermolecular interactions occur between dye and PAL. The N-3 sample shows the optimal adsorp- tion capacity which is evidently higher than raw PAL, and the N-3 sample can thoroughly remove the MB from the 200 mg/L of solution at the dosage of 2 g/L (Scheme 1), but the raw PAL fails to decolor the MB solution, which confirms that the generation of more adsorption sites on PAL after alkali activation is very favorable to the removal of cationic dye. For raw PAL, the adsorption process is mainly involved with the weaker electrostatic interaction between the low-charge-density surface of PAL and MB, the hydrogen bonding between Si–OH and the C–N moiety of MB, and the pore adsorption. After activation, the negative surface charge density of PAL greatly increased and more –Si–O^- groups were formed due to the breakage of Si–O–Si and Si–O–M bonds, which are very beneficial to greatly strengthen the electrostatic interaction, and new complexing or association interactions between PAL and MB could be generated, which means that more "hands" in activated PAL than raw PAL are available to "grasp" MB molecules from aqueous solution and remove them (Scheme 1).

3.2.3 Adsorption Kinetics

Adsorption rate is especially important for the practical application of an adsorbent. As is shown in Fig. 10, the adsorption amount of PAL samples for MB rapidly increased with prolonging the contact time *t* (s), and the adsorption equilibrium can be reached within 30 min. In order to explore the adsorption mechanism, mass transfer, and chemical reaction, the pseudo-first-order (Eq. 6) and pseudo-second-order (Eq. 7) kinetic equations were employed to fit the adsorption data (Rudzinsk and Plazinski 2006):

$$log(q_e - q_t) = logq_e - (k_1/2.303)t \quad (6)$$

$$t/q_t = 1/k_2 q_e^2 + t/q_e \quad (7)$$

where q_e and q_t are the adsorption capacities of PAL samples for MB (mg/g) at equilibrium and at time *t* (s), respectively. k_1 is the pseudo-first-order rate constant

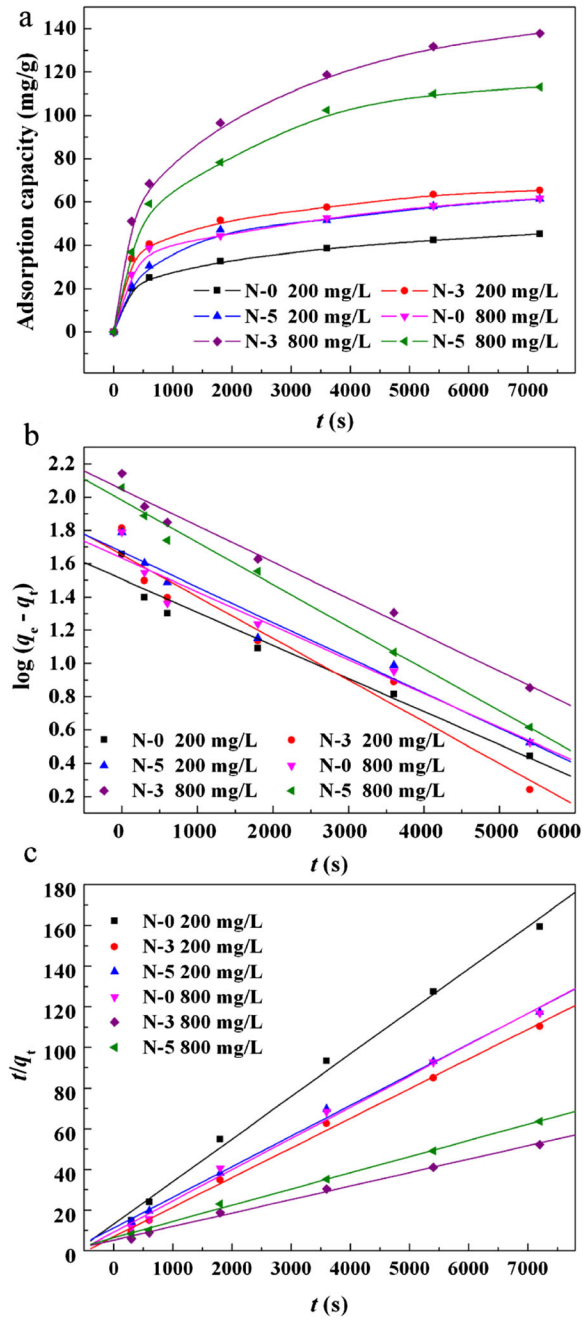

Fig. 10 Adsorption kinetic curves of PAL samples at different initial concentrations of MB (**a**) and the fitting curves by pseudo-first-order kinetic model (**b**) and pseudo second-order kinetic model (**c**)

(s^{-1}), and k_2 is the pseudo-second-order rate constant (mg/g/s). k_1 and k_2 values can be calculated by the slope and intercept from the straight lines of $\log(q_e - q_t)$ vs *t* and t/q_t *vs t*, respectively (Table 3). The initial adsorption rate constant k_{2i} (mg/g/s) is equal to $k_2 q_e^2$ (Table 3).

Table 3 Adsorption kinetic parameters for the adsorption of MB onto PAL

	Pseudo-first-order model				Pseudo-second-order model			
	$q_{e,\ exp}$ (mg/g)	$q_{e,\ cal}$ (mg/g)	$k_1\times10^4$ (s^{-1})	R	$q_{e,\ cal}$ (mg/g)	$k_2\times10^5$ g/(mg s)	k_{2i} mg/(g s)	R
N-0 (200 mg/L)	45.16	32.10	4.5839	0.9812	47.58	3.3248	0.0761	0.9975
N-3 (200 mg/L)	65.30	44.86	5.7716	0.9763	68.59	3.1180	0.1467	0.9986
N-5 (200 mg/L)	61.37	46.85	4.8836	0.9802	66.36	2.0259	0.0892	0.9984
N-0 (800 mg/L)	61.65	42.89	4.6806	0.9741	65.11	2.5815	0.1094	0.9971
N-3 (800 mg/L)	137.93	111.28	5.0366	0.9919	145.60	0.8443	0.1915	0.9981
N-5 (800 mg/L)	113.12	95.63	5.8313	0.9950	120.31	0.9965	0.1565	0.9986

As can be seen, the theoretical q_e values obtained by pseudo-first-order kinetic model are far from the experimental values. However, the q_e values calculated from pseudo-second-order model are almost equal to the experimental values with the correlation coefficient (R) larger than 0.9971, indicating that the pseudo-second-order kinetic model can describe the adsorption kinetics very well and the adsorption of PAL for MB is probably controlled by the external mass transfer and intraparticle diffusion. From Table 3, it was found that the initial adsorption rate of the PAL samples for MB follows the order N-3>N-5>N-0 for both the initial MB concentrations of 200 and 800 mg/L. With increasing the initial concentration, the adsorption rate of each sample was clearly enhanced.

3.2.4 Sustainable Utilization of PAL After Adsorption

The reutilization of used adsorbents has becoming a hot topic in recent years. What is encouraging is that the MB-loaded PAL is highly resistant to HCl solution, NaOH solution, and organic solvents. As shown in Fig 11, the MB-loaded PAL shows bright blue color. After being treated with 0.2 mol/L HCl solution, the color of used adsorbents is still remained. Similarly, the color of MB-loaded PAL has no obvious change after being treated with 0.2 mol/L NaOH solution, anhydrous ethanol, acetone, and dimethyl formamide (DMF). As is previously reported (Polette-Niewold et al. 2007), PAL has been used as irreplaceable raw material to fabricate organic–inorganic hybrid pigments, such as Maya blue. Here, the enhanced adsorption of MB onto PAL by moderate alkali activation is found to be favorable to fabricate stable hybrid pigment for potential applications in the paint and pigment industry. Thus, the present study provides not only an experimental foundation for the removal of dye from wastewater, but also a simultaneous method of synthesizing hybrid pigments.

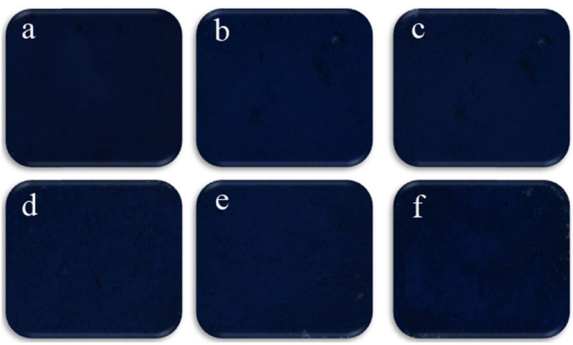

Fig. 11 Digital photographs of the MB-loaded activated PAL (**a**) and after desorbed by **b** 0.2 mol/L of HCl solution, **c** 0.2 mol/L of NaOH solution, **d** anhydrous ethanol, **e** acetone, and **f** DMF

4 Conclusions

Alkali activation has been successfully introduced to enhance the adsorption capacity of PAL for MB. It was found that the metal ions in the crystal backbone of PAL could be selectively removed by controlling the concentration of alkali solution. Interestingly, apart from the acid activation, the Si–O–M and Si–O–Si bonds were moderately broken in the alkali activation process, with new adsorption sites to be built. This effectively increases the surface negative potential of PAL and enhances the adsorption properties for MB. The nanorod-like crystal of PAL became shorter after alkali activation at the relatively lower concentration (<5 mol/L). The rod-like morphology and BET specific surface area of PAL almost disappeared when it was attached by the relatively higher concentration of NaOH

solution (i.e., 5.0 mol/L), which implies that the pore structure collapsed. Although the specific surface area of PAL activated by 5 mol/L of NaOH solution is almost equal to zero, it still owns a far better adsorption capacity than raw PAL. It could be inferred from the above analysis that the adsorption is not primarily affected by specific surface area, but by the interactions, e.g., electrostatic, complexing, and hydrogen bonding. The activated PAL may fade the MB solution (200 mg/L), which is greatly superior to the raw PAL. Another surprise was found to be that the MB-loaded PAL shows higher stability and could be used to produce Maya blue-like pigment, which provides a new approach for the sustainable utilization of PAL adsorbents.

Acknowledgment The authors would like to thank "863" Project of the Ministry of Science and Technology, People's Republic of China (No. 2013AA032003), the National Natural Science Foundation of China (No. 51403221), and the open funds of Key Laboratory for Palygorskite Science and Applied Technology of Jiangsu Province (No. HPK201201).

References

Al-Futaisi, A., Jamrah, A., & Al-Hanai, R. (2007). Aspects of cationic dye molecule adsorption to palygorskite. *Desalination, 214*, 327–342.

Bakandritsos, A., Steriotis, T., & Petridis, D. (2004). High surface area montmorillonite-carbon composites and derived carbons. *Chemistry of Materials, 16*, 1551–1559.

Barrett, E. P., Joyner, L. G., & Halenda, P. P. (1951). Study of pore size distribution by capillary absorption method. *Journal of the American Chemical Society, 73*, 373–380.

Barrios, M. S., Gonzalez, L. V., Rodriguez, M. A., & Pozas, J. M. (1995). Acid activation of a palygorskite with HCl: development of physico-chemical, textural and surface properties. *Applied Clay Science, 10*, 247–258.

Bradley, W. D. (1940). The structural scheme of attapulgite. *American Mineralogist, 25*, 405–410.

Bu, X. Z., Zhang, G. K., Gao, Y. Y., & Yang, Y. Q. (2010). Preparation and photocatalytic properties of visible light responsive N-doped TiO_2/rectorite composites. *Microporous Mesoporous Materials, 136*, 132–137.

Chen, H., Zhao, Y. G., & Wang, A. Q. (2007). Removal of Cu (II) from aqueous solution by adsorption onto acid-activated palygorskite. *Journal of Hazardous Materials, 149*, 346–354.

Çöle, G., Gök, M. K., & Güçlü, G. (2013). Removal of basic dye from aqueous solutions using a novel nanocomposite hydrogel: *N*-vinyl 2-pyrrolidone/itaconic acid/organo clay. *Water, Air, & Soil Pollution, 224*, 1760.

Freundlich, H. M. F. (1906). Über die adsorption in lösungen. *Zeitschrift für Physikalische, 57*, 385.

Frini-Srasra, N., & Srasra, E. (2010). Acid treatment of south Tunisian palygorskite: removal of Cd(II) from aqueous and phosphoric acid solutions. *Desalination, 250*, 26–34.

Frost, R. L., Xi, Y. F., & He, H. P. (2010). Synthesis, characterization of palygorskite supported zero-valent iron and its application for methylene blue adsorption. *Journal of Colloid and Interface Science, 341*, 153–161.

Galan, E. (1996). Properties and applications of palygorskite and sepiolite. *Clays and Clay Minerals, 31*, 443–453.

Golden, D. C., Dixon, J. B., Shadfan, H., & Kippenberger, L. A. (1985). Palygorskite and sepiolite alteration to smectite under alkaline conditions. *Clays and Clay Minerals, 33*, 44–50.

Gonzalez, F., Pesquera, C., Blanco, C., Benito, I., Mendioroz, S., & Pajares, J. A. (1990). Structural and textural evolution under thermal treatment of natural and acid-activated Al-rich and Mg-rich palygorskites. *Applied Clay Science, 5*, 23–36.

Grabowska, E. L., & Gryglewicz, G. (2007). Adsorption characteristics of Congo Red on coal-based mesoporous activated carbon. *Dyes and Pigments, 74*, 34–40.

Jozefaciuk, G., & Bowanko, G. (2002). Effect of acid and alkali treatments on surface areas and adsorption energies of selected minerals. *Clays and Clay Minerals, 50*, 771–783.

Jozefaciuk, G., & Matyka-Sarzynska, D. (2006). Effect of acid treatment and alkali treatment on nanopore properties of selected minerals. *Clays and Clay Minerals, 54*, 220–229.

Kumar, K. Y., Muralidhara, H. B., Nayaka, Y. A., Balasubramanyama, J., & Hanumanthappa, H. (2013). Low-cost synthesis of metal oxide nanoparticles and their application in adsorption of commercial dye and heavy metal ion in aqueous solution. *Powder Technology, 246*, 125–136.

Langmuir, I. (1918). The adsorption of gases on plane surfaces of glass, mica and platinum. *Journal of the American Chemical Society, 40*, 1361–1403.

Liu, Y., Wang, W. B., & Wang, A. Q. (2012). Effect of dry grinding on the microstructure of palygorskite and adsorption efficiency for methylene blue. *Powder Technology, 225*, 124–129.

Liu, H. B., Chen, T. H., Chang, D. Y., Chen, D., Qing, C. S., Xie, J. J., & Frost, R. L. (2013). The difference of thermal stability between Fe-substituted palygorskite and Al-rich palygorskite. *Journal of Thermal Analysis and Calorimetry, 111*, 409–415.

McKeown, D. A., Post, J. E., & Etz, E. S. (2002). Vibrational analysis of palygorskite and sepiolite. *Clays and Clay Minerals, 50*, 667–680.

Middea, A., Fernandes, T. L. A. P., Neumann, R., da Gomes, O. F. M., & Spinelli, L. S. (2013). Evaluation of Fe(III) adsorption onto palygorskite surfaces. *Applied Surface Science, 282*, 253–258.

Olu-Owolabi, B. I., Popoola, D. B., & Unuabonah, E. I. (2010). Removal of Cu^{2+} and Cd^{2+} from aqueous solution by bentonite clay modified with binary mixture of goethite and humic acid. *Water, Air, & Soil Pollution, 211*, 459–474.

Papoulis, D., Komarneni, S., Panagiotaras, D., Stathatos, E., Toli, D., Christoforidis, K. C., Fernández-García, M., Li, H. H., Yin, S., Sato, T., & Katsuki, H. (2013a). Halloysite–TiO_2 nanocomposites: synthesis, characterization and photocatalytic activity. *Applied Catalysis B: Environmental, 132–133*, 416–422.

Papoulis, D., Komarneni, S., Panagiotaras, D., Tsolis-Katagas, P., Panagiotaras, D., Kacandes, H. G., Zhang, P., Yin, S., Sato,

T., & Katsuki, H. (2013b). Palygorskite–TiO_2 nanocomposites: part 1. Synthesis and characterization. *Applied Clay Science, 83*, 191–197.

Post, J. E., Heaney, P. J. (2008). Synchrotron powder X-ray diffraction study of the structure and dehydration behavior of palygorskite. *American Mineralogist, 93*, 667–675.

Polette-Niewold, L. A., Manciu, F. S., Torres, B., Jr., Alvarado, M., & Chianelli, R. R. (2007). Organic/inorganic complex pigments: ancient colors maya blue. *Journal of Inorganic and Biochemistry, 101*, 1958–1973.

Rouquerol, F., Rouquerol, J., & Sing, K. (1999). *Adsorption by powders and porous solids: principles, methodology and applications*. London: Academic Press.

Rudzinsk, W., & Plazinski, W. (2006). Kinetics of solute adsorption at solid/solution interfaces: a theoretical development of the empirical pseudo-first and pseudo-second order kinetic rate equations, based on applying the statistical rate theory of interfacial transport. *Journal of Physical Chemistry B, 110*, 16514–16525.

Ruiz-Hitzky, E., Darder, M., Fernandes, F. M., Wicklein, B., Alcântara, A. C. S., & Aranda, P. (2013). Fibrous clays based bionanocomposites. *Progress in Polymer Science, 38*, 1392–1414.

Sarkar, B., Megharaj, M., Xi, Y. F., & Naidu, R. (2012). Surface charge characteristics of organo-palygorskites and adsorption of p-nitrophenol in flow-through reactor system. *Chemical Engineering Journal, 185–186*, 35–43.

Sánchez del Río, M., Boccaleri, E., Milanesio, M., Croce, G., van Beek, W., Tsiantos, C., et al. (2009). A combined synchrotron powder diffraction and vibrational study of the thermal treatment of palygorskite–indigo to produce Maya blue. *Journal of Materials Science, 44*, 5524–5536.

Sing, K. S. W., Everett, D. H., Haul, R. A. W., Moscou, L., Pierotti, R. A., Rouquerol, J., & Siemieniewska, T. (1985). Physical and biophysical chemistry division commission on colloid and surface chemistry including catalysis. *Pure and Applied Chemistry, 57*, 603–619.

Sotelo, J. L., Ovejero, G., Rodríguez, A., Álvarez, S., & García, J. (2013). Study of natural clay adsorbent sepiolite for the removal of caffeine from aqueous solutions: batch and fixed-bed column operation. *Water, Air, & Soil Pollution, 224*, 1466.

Suárez, M., & Garcia-Romero, E. (2006). FTIR spectroscopic study of palygorskite: influence of the composition of the octahedral sheet. *Applied Clay Science, 31*, 154–163.

Szabó, E., Simon, G., Dombi, A., Hernádi, K., Baia, L., & Pap, Z. (2014). Important aspects on the removal of humic acid and phenolic compounds with clay minerals. "Synergism provided by the pollutants, efficiency given by the media". *Water, Air, & Soil Pollution, 225*(3), 1–10.

Wan Ngah, W. S., Teong, L. C., & Hanafiah, M. (2011). Adsorption of dyes and heavy metal ions by chitosan composites: a review. *Carbohydrate Polymers, 83*, 1446–1456.

Wang, W. B., Huang, D. J., Kang, Y. R., & Wang, A. Q. (2013). One-step in-situ fabrication of a granular semi-IPN hydrogel based on chitosan and gelatin for fast and efficient adsorption of Cu^{2+} ion. *Colloids and Surface B, 106*, 51–59.

Wang, B., Zhang, G. X., Sun, Z. M., & Zheng, S. L. (2014). Synthesis of natural porous minerals supported TiO_2 nanoparticles and their photocatalytic performance towards Rhodamine B degradation. *Powder Technology, 262*, 1–8.

White, R. D., Bavykin, D. V., & Walsh, F. C. (2012). The stability of halloysite nanotubes in acidic and alkaline aqueous suspensions. *Nanotechnology, 23*, 065705 (10 pp).

Xu, J. X., Wang, W. B., Wang, A. Q., & Zheng, M. S. (2014). Dispersion of palygorskite in ethanol-water mixtures via high-pressure homogenization: microstructure and colloidal properties. *Powder Technology, 261*, 98–104.

Yan, W., Liu, D., Tan, D., Yuan, P., & Chen, M. (2012). FTIR spectroscopy study of the structure changes of palygorskite under heating. *Spectrochimica Acta Part A: Molecular and Biomolecular Spectroscopy, 97*, 1052–1057.

Zhang, J. P., Wang, Q., Chen, H., & Wang, A. Q. (2010). XRF and nitrogen adsorption studies of acid-activated palygorskite. *Clay Minerals, 45*, 145–156.

Zhang, J., Cai, D., Zhang, G., Cai, C., Zhang, C., Qiu, G., & Wu, Z. (2013). Adsorption of methylene blue from aqueous solution onto multiporous palygorskite modified by ion beam bombardment: effect of contact time, temperature, pH and ionic strength. *Applied Clay Science, 83*, 137–143.

Zhang, Y., Wang, W. B., Zhang, J. P., Liu, P., & Wang, A. Q. (2015). A comparative study about adsorption of natural palygorskite for methylene blue. *Chemical Engineering Journal, 262*, 390–398.